International Journal of Minerals, Metallurgy and Materials
Volume 19, Number 8, Aug 2012, Page 768
DOI: 10.1007/s12613-012-0626-y

Structure and properties of NASICON synthesized by two different zirconium salts

Heng-yao Dang, Xing-min Guo, Yong-ping Huang, and Jiang-qi Rong

Department of Physical Chemistry, School of Metallurgical and Ecological Engineering, University of Science and Technology Beijing, Beijing 100083, China

(Received: 19 October 2011; revised: 14 February 2012; accepted: 21 February 2012)

Abstract: $ZrOCl_2 \cdot 8H_2O$ and $ZrO(NO_3)_2 \cdot 2H_2O$ were used respectively to synthesize a NASICON solid electrolyte by a sol-gel method. The structure and properties of two samples were characterized by X-ray diffraction (XRD), scanning electron microscopy (SEM), and electrochemical impedance spectroscopy (EIS). The crystal structure was investigated by the Rietveld refinement. It is found that both the samples contain a monoclinic $C2/c$ phase as the main conductive phase with the lattice parameters of a=1.56312 nm, b=0.90784 nm and c=0.92203 nm, though a small amount of rhombohedral phase is also detected in the final product. The sample synthesized by $ZrO(NO_3)_2 \cdot 2H_2O$ contains more monoclinic phase (89.48wt%) than that synthesized by $ZrOCl_2 \cdot 8H_2O$ (74.91wt%). As expected, the ionic conductivity of the latter is higher than that of the former; however, the activation energy of the latter (0.37 eV) is slightly higher than that of the former (0.35 eV).

Keywords: NASICON; superionic conducting materials; sodium compounds; sol-gel process; microstructure; electrical conductivity

[*This work was partly supported by the National Natural Science Foundation of China (No.50974012) and Program Changjiang Scholars and Innovative Research Team in Universities (No.0708).*]

1. Introduction

Sodium super-ionic conductors (NASICON) with the general formula $Na_{1+x}Zr_2Si_xP_{3-x}O_{12}$ ($0 \leq x \leq 3$) were first synthesized by Hong [1] and Goodenough *et al.* [2]. The NASICON structure has rhombohedral symmetry, except in the interval $1.8 \leq x \leq 2.2$, where small distortion to monoclinic symmetry takes place. The highest ionic conductivity is observed in the monoclinic structure obtained for x=2.0 and close to that of β-alumina, which has two-dimensional ionic mobility. A compound $Na_3Zr_2Si_2PO_{12}$ has a structure made by a three-dimensional framework of SiO_4/PO_4 tetrahedra corners sharing with ZrO_6 octahedra, in which Na^+ ions occupy the interstitial sites. Ionic conduction takes place when Na^+ ions move from one site to another through "bottlenecks" formed by oxygen ions. NASICON with nominal composition $Na_3Zr_2Si_2PO_{12}$ has attracted more and more attention for promising use in solid-state electrochemical devices. Especially, it has been emphasized for the preparation of CO_2 electrochemical sensors [3-7].

The NASICON material is usually synthesized by two methods (the traditional solid state reaction and sol-gel method), which affect the microstructure of samples [8-9]. The solid state method requires a higher temperature leading to the volatilization of Na_2O and P_2O_5 and the resultant segregation of zirconia at the grain boundary, which causes a decrease in ionic conductivity. A reduced sintering temperature seems to be advantageous for obtaining a desired composition. The newly developed metal-organic sol-gel procedure has overcome the problems, but the raw material is very expensive, and thus limits the method to be extensively applied [10]. Subsequently, some inorganic metal salts such as $ZrOCl_2 \cdot 8H_2O$ or $ZrO(NO_3)_2 \cdot 2H_2O$ were used as a substitute for metal-organic [11-13]. However, there is little information about the difference in the microstructure and electrical properties of NASICON synthesized by two

Corresponding author: Xing-min Guo E-mail: guoxm@ustb.edu.cn

kinds of zirconium salts in literatures.

In the present work, we have prepared the NASICON material using a sol-gel method with two different zirconium salts mentioned above and compared the difference in the microstructure and electrical properties.

2. Experimental

2.1. Synthesis of the NASICON material

The NASICON material was synthesized by a sol-gel method [14]. $ZrOCl_2·8H_2O$ was used as main raw materials and the preparation process is shown in Fig. 1. $ZrOCl_2·8H_2O$ was dissolved in deionized water to form an aqueous solution first. The, NH_4OH was added to the above solution dropwise under stirring. The complete precipitation of $ZrO(OH)_2$ was realized by controlling the pH value of the solution above 7.2. The purified $ZrO(OH)_2$ was dissolved into an aqueous solution of nitric acid after Cl^- was eliminated by washing away iteratively. The solution was stirred at 50°C for 0.5 h to get a clear solution of $Zr(NO_3)_4$. The silica sol was prepared in a molar ratio of $[H_2O]/[C_2H_5OH]/[Si(OC_2H_5)_4]=0.717:0.717:1$ and added into the previous solution. Finally, a $Na_3PO_4·12H_2O$ aqueous solution was quickly added as the required proportion. The mixture was stirred to form a sol and then dried at 80°C for 24 h to form a xerogel. The xerogel was ball milled into fine powders and then pre-calcined at 500°C for 0.5 h in air to remove organic compounds. Then the resulted NASICON precursor powders were formed into pellets under the uniaxial pressure of 50 kN. Sintering was done at 900°C for 2 h. In the case of $ZrO(NO_3)_2·2H_2O$ used as a raw material, the preparation process is similar to that of $ZrOCl_2·8H_2O$. Compared with $ZrOCl_2·8H_2O$, NASICON synthesized by $ZrO(NO_3)_2·2H_2O$ is far simpler because Cl^- is nonexistent in the raw material. The preparation process has been described in detail in our previous work [15]. NASICON samples synthesized using $ZrOCl_2·8H_2O$ and $ZrO(NO_3)_2·2H_2O$ as main raw materials are indicated as sample A and sample B, respectively.

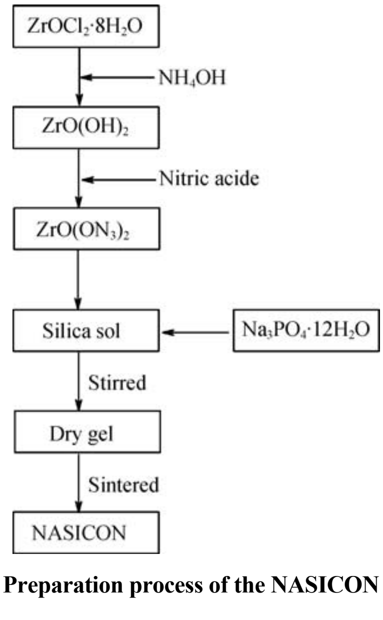

Fig. 1. Preparation process of the NASICON material.

2.2. Measurements

X-ray diffraction (XRD, by MXP21VAHF, MAC Seience Co. Ltd. JPN) and scanning electron microscopy (SEM, by JSM-6480LV, JEOL Ltd. JPN) were used to determine the composition and microstructural properties of the prepared pellets. To further confirm the crystal structure, the Rietveld refinement was employed using the FULLProf computer tools. The density of pellets was measured by the Archimedes method with ethanol as an immersion medium. Electrical properties were determined based on electrochemical impedance spectroscopy (EIS) measurements in the frequency range of 0.01-10^5 Hz between 200 and 400°C in air. The amplitude of sinusoidal voltage was 5 mV. The sample was allowed to equilibrate for 2 h before measurements. Prior to the measurements, two flat surfaces of the NASICON pellets were polished and a pair of Pt electrodes was deposited by screen-printing on both flat sides of the pellets.

2.3. Equivalent circuit model

Electrochemical impedance spectroscopy is a powerful technique for unraveling the electrical properties of an electrolyte [16]. It enables the overall electrical properties of the electrolyte material to be separated into their components, which can then be systematically studied or modified. Frequently, experiment is carried out over a wide frequency range (0.01-10^5 Hz in our present experiment as mentioned above), and the interpretation of the resulting spectra is aided by analogy to equivalent circuits involving simple components such as resistors, capacitors and some other elements. Normally, impedance data are presented in the Nyquist ($-\mathrm{Im}Z$ *vs.* $\mathrm{Re}Z$) form. A good correspondence between experimental data and fitted curves is then taken as a confirmation that the proposed circuit provides a good description of the system under investigation. Here an equivalent circuit model with explicit physical meaning is proposed as shown in Fig. 2. In Fig. 2, R_b is the resistance of the bulk; C_{gb} and R_{gb} represent the capacitance and resistance of grain boundaries, respectively; C_{dl} and R_{ct} are the double layer capacitance and the charge transfer resistance of electrodes, respectively; and Q is the constant phase element

(CPE) related to the ions diffusion process. The adapted equivalent circuit is finally used to fit our experimental impedance data.

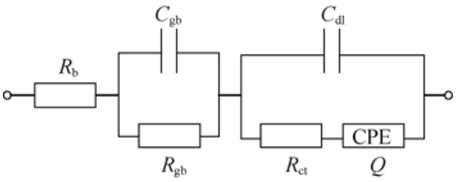

Fig. 2. Equivalent circuit for simulating the impedance spectra of two samples.

3. Results and discussions

3.1. Density and microstructure

The densities of the samples were measured based on the Archimedes law. The results are listed in Table 1. Sample B has the density of 2.71 $g\cdot cm^{-3}$, which is much lower than that of sample A (2.96 $g\cdot cm^{-3}$, close to the theoretical value of 3.26 $g\cdot cm^{-3}$). This may be caused by the bigger volumetric shrinkage of sample A (32.9%) than that of sample B (6.78%). Furthermore, the true porosity of sample B (16.85%) is far larger than that of sample A. Both the values of density and porosity seem to suggest that using $ZrOCl_2\cdot 8H_2O$ as the main raw material is helpful to enhance the densification of NASICON sintered pellets.

Fig. 3 illustrates the surface microstructure observed by SEM for the two samples. An obvious difference in the microstructures was observed. There are lots of pores in sample B synthesized by $ZrO(NO_3)_2\cdot 2H_2O$ with a rough surface, while the surface of sample A is relatively smooth and dense. These findings are consistent with that discussed above.

Table 1. Values of density and porosity of two investigated NASICON samples

Sample.	Volume density / ($g\cdot cm^{-3}$)	Relative density / %	Volumetric shrinkage / %	True porosity / %	Apparent porosity / %	Closed porosity / %
A	2.96	90.80	32.90	9.23	1.61	7.62
B	2.71	83.13	6.78	16.85	14.00	2.85

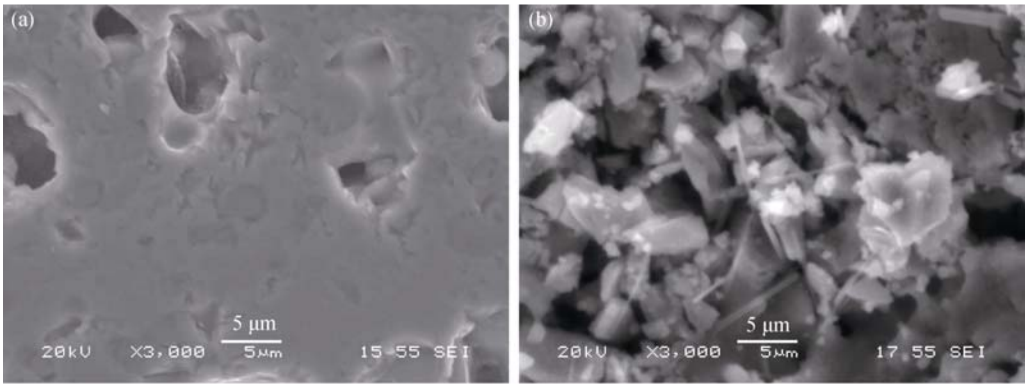

Fig. 3. SEM photographs of samples A (a) and B (b).

The XRD patterns of the two samples are shown in Fig. 4. It is worth noting that there is no ZrO_2 phase appearing in both the samples, which tends to appear easily in the normal high-temperature solid-state reaction process [17-19]. The XRD patters of both the samples are almost the same while the crystallization degrees are different. It is believed that the crystallization degree of sample A is better than that of sample B because the XRD peaks of sample A are sharper and narrower than those of the sample B, as shown in Fig. 4. To further confirm the crystal structure, the Rietveld method was employed. The main crystal phase in both the samples is identified in the monoclinic system of $C2/c$ space group, although small amount of rhombohedral phase ($R\overline{3}c$) is also detected in the final product. The refined cell parameters are a=1.56312 nm, b=0.90784 nm and c=0.92203 nm, which are in good agreement with the values reported by Hong [1]. The main difference is that sample B contained more monoclinic phase (89.48wt%) as the main conductive phase [8] than sample A (74.91wt%). It seems to imply that sample B is expected to have a higher conductivity than the sample A.

3.2. Electrical conductivity

The electrical properties of the NASICON samples were measured by EIS, which allowed distinguishing the resistances of the bulk and the grain boundary for a polycrystal-

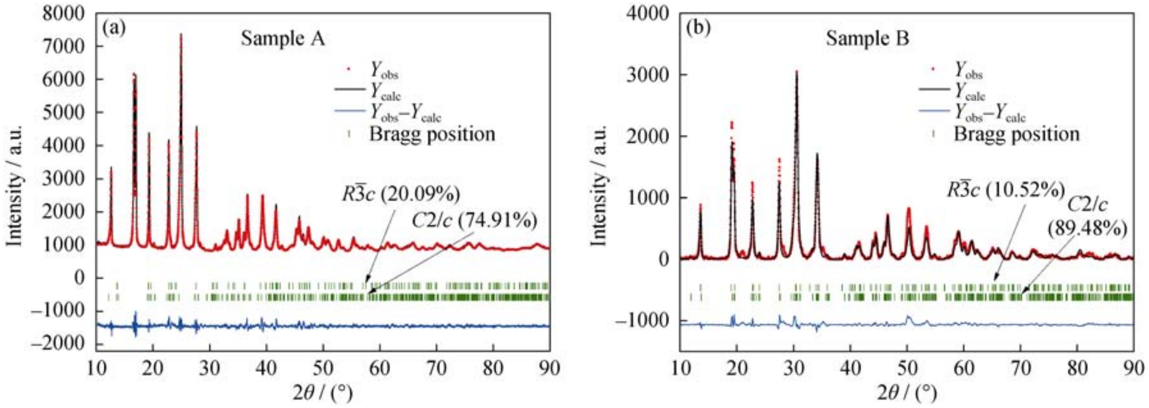

Fig. 4. XRD patterns and their Rietveld refinement results of samples A (a) and B (b).

line electrolyte. The Nyquist diagrams of the two samples are shown in Fig. 5. The geometrical shape of the impedance spectra of both the samples is similar. The contribution described at low frequencies characterizes the response of the NASICON/Pt electrode interface. The spectra observed at mediate frequencies translate the blocking effect of charge carriers at the grain boundaries. At high frequencies, the impedance diagram corresponds to the specific response of the bulk. In this present experiment, the impedance data were recorded at higher temperatures. Consequently, the semicircle corresponding to the bulk impedance is out with respect to the frequency scale of the instrumentation. Normally, the resistance of grains in the samples can be obtained at the intersection point of the spectra with the real axis at high frequencies. The correspondence between experimental data and fitted curves obtained with the equivalent circuit (Fig. 2) is excellent over the whole frequency and temperature range measured, implying the model is a reasonable explanation for the spectra. The impedance parameters were derived from the spectra by fitting the data to an equivalent circuit using complex nonlinear least square (CNLS) fitting techniques.

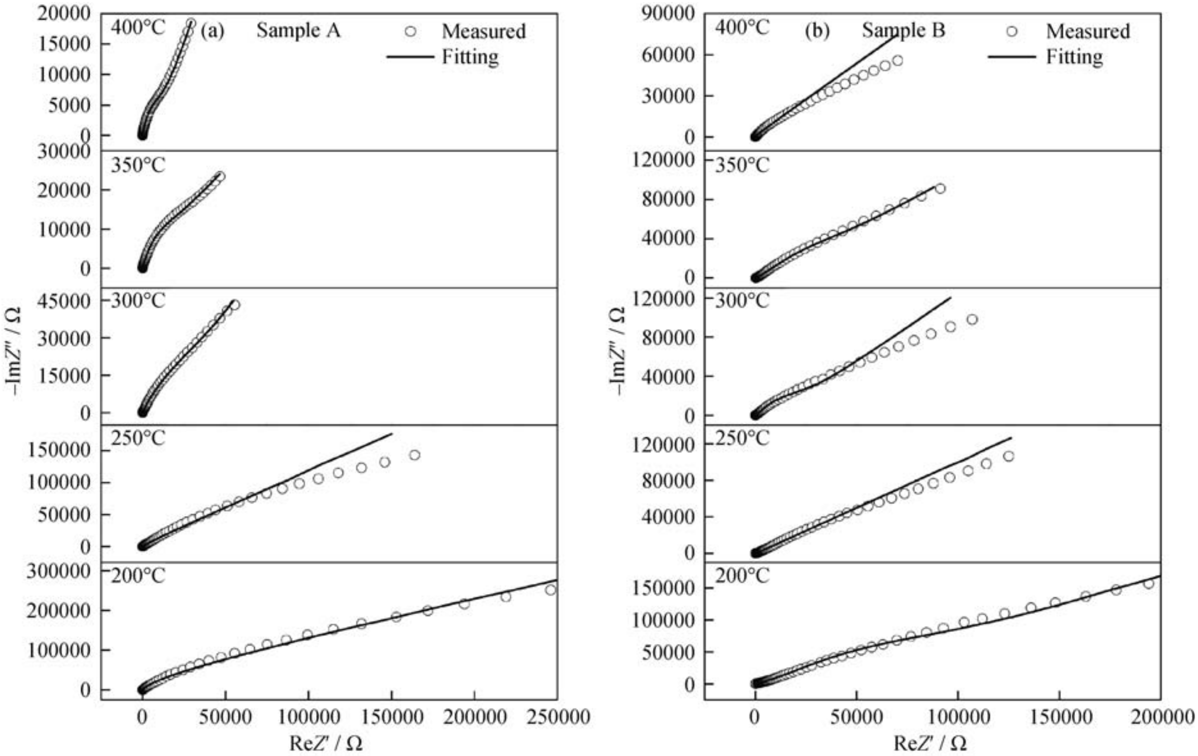

Fig. 5. Impedance diagrams in Nyquist coordinates of samples A (a) and B (b). Solid lines represent CNLS fitting to the equivalent circuit at different temperatures.

The conductivity of both the samples is given by

$$\sigma = \frac{4l}{\pi D^2 R} \tag{1}$$

where D and l are the diameter and the thickness of the two samples respectively, and R is the resistance of the bulk given by the above fitting results. The ionic conductivities of samples A and B at 300°C are 0.32 $S \cdot cm^{-1}$ and 0.48 $S \cdot cm^{-1}$, respectively, which are in the same order of magnitude compared with results reported by Andersen *et al.* [20] at the same temperature. Furthermore, the activation energy (E_a) of Na^+ ion migration in both the samples is given by the Arrhenius equation as follows:

$$\sigma = \frac{\sigma_0}{T} \exp\left(-\frac{E_a}{kT}\right) \tag{2}$$

where σ_0 is the pre-exponential factor, T is the temperature in Kelvin, k is the Boltzmann's constant. While the natural logarithm is taken to Eq.(2), it can be transformed into

$$\ln(\sigma T) = \ln \sigma_0 - \frac{E_a}{k} \frac{1}{T} \tag{3}$$

Thus, $\ln(\sigma T)$ is linear to $1/T$ with a slope of E_a/k. The evolution of conductivity in the Arrhenius plot is represented in Fig. 6. As shown in this figure, the relationship between the conductivity and temperature is in good agreement with the Arrhenius relationship for both the samples. The activation energy of Na^+ ion migration in the samples is determined from the slope of the fitted straight line. The conductivity of the two samples increases with increasing temperature. As expected, the conductivity of sample B is higher than that of sample A. The finding is consistent with the expected by examining the Rietveld refinement results. On the other hand, for sample B, the activation energy of Na^+ ion migration (0.37 eV) is slightly higher than that of sample A (0.35 eV). The results of activation energy are very close to the values reported in other literatures [21-23].

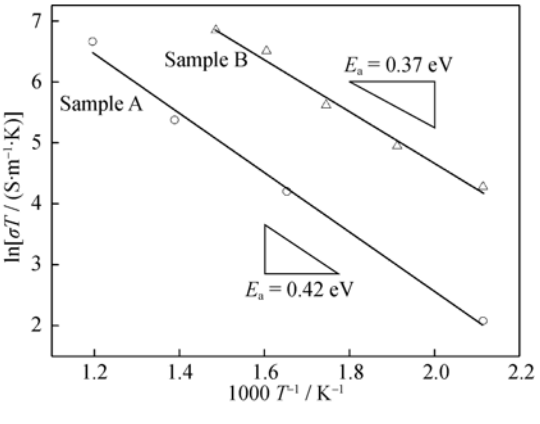

Fig. 6. Arrhenius plots of the samples.

4. Conclusions

$ZrOCl_2 \cdot 8H_2O$ and $ZrO(NO_3)_2 \cdot 2H_2O$ were used as the main raw materials respectively to synthesize NASICON solid electrolyte materials by a sol-gel method. Compared with the sample synthesized by $ZrO(NO_3)_2 \cdot 2H_2O$, the sample synthesized by $ZrOCl_2 \cdot 8H_2O$ shows to be more dense with a density of 2.96 $g \cdot cm^{-3}$, being close to the theoretical value. As revealed by the Rietveld refinement result, both the samples contain a monoclinic system of $C2/c$ space group as the major crystalline phase with cell parameters a=1.56312 nm, b=0.90784 nm, and c=0.92203 nm, though a small amount of rhombohedral phase is also detected in the final product. However, sample B contains more monoclinic structure (89.48wt%) than sample A (74.91wt%). As expected, the ionic conductivity of sample B is higher than that of sample A. As for the activation energy of Na^+ ion migration, sample B (0.37 eV) is slightly higher than sample A (0.35 eV), which is closely related to its microstructure of high porosity.

References

[1] H.Y.P. Hong, Crystal structures and crystal chemistry in the system $Na_{1+x}Zr_2Si_xP_{3-x}O_{12}$, *Mater. Res. Bull.*, 11(1976), No.2, p.173.

[2] J.B Goodenough, H.Y.P. Hong, and J.A. Kafalas, Fast Na^+-ion transport in skeleton structure, *Mater. Res. Bull.*, 11(1976), No.2, p.203.

[3] D. Zhu, F. Luo, Z. Xie, and W. Zhou, Preparation and characteristic of NASICON ceramics, *Rare Met.,* 25(2006), No.6, p.39.

[4] M. Morio, T. Hyodo, Y. Shimizu, and M. Egashira, Effect of macrostructural control of an auxiliary layer on the CO_2 sensing properties of NASICON-based gas sensors, *Sens. Actuators B*, 139(2009), No.2, p.563.

[5] T. Kida, M.H. Seo, S. Kishi, Y. Kanmura, N. Yamazoe, and K. Shimanoe, Application of a solid electrolyte CO_2 sensor for the analysis of standard volatile organic compound gases, *Anal. Chem.*, 82(2010), No.8, p.3315.

[6] T. Kida, S. Kishi, N. Yamazoe, and K. Shimanoe, Stability and interfacial structure of a NASICON-based CO_2 sensor fitted with a solid-reference electrode, *Sens. Lett.*, 9(2011), No.1, p.288.

[7] T. Kida, N. Morinaga, S. Kishi, K.M. An, K.W. Sim, B.Y. Chae, J.K. Kim, B.K. Ryu, and K. Shimanoe, Electrochemical detection of volatile organic compounds using a $Na_3Zr_2Si_2PO_{12}/Bi_2Cu_{0.1}V_{0.9}O_{5.35}$ heterojunction device, *Electrochim. Acta*, 56(2011), No.22, p.7484.

[8] U. von Alpen, M.F. Bell, and W. Wichelhaus, Phase

transition in NASICON ($Na_3Zr_2Si_2PO_{12}$), *Mater. Res. Bull.*, 14(1979), No.10, p.1317.

[9] B.E. Yoldas and I.K. Lloyd, Nasicon formation by chemical polymerization, *Mater. Res. Bull.*, 18(1983), No.10, p.1171.

[10] Y. Yang and C.C. Liu, Development of a NASICON-based amperometric carbon dioxide sensor, *Sens. Actuators B*, 62(2000), No.1, p.30.

[11] Y. He, B. Quan, B. Wang, C. Zhang, and F. Liu, Investigation of miniature CO_2 gas sensor based on NASICON, *Russ. J. Electrochem.*, 43(2007), No.11, p.1289.

[12] B. Wang, X.S. Liang, F.M. Liu, T.G. Zhong, C. Zhao, G.Y. Lu, and B.F. Quan, Synthesis and characterization of NASICON nanoparticles by sol-gel method, *Chem. Res. Chin. Univ.*, 25(2009), No.1, p.13.

[13] X.S. Liang, S.Q. Yang, T.G. Zhong, Q. Diao, H. Zhang, J.G. Li, B.F. Quan, and G.Y. Lu, Mixed potential type carbon monoxide sensor utilizing NASICON and spinel type oxide electrode, *Sens. Lett.*, 9(2011), No.2, p.832.

[14] S. Zhang, B.F. Quan, Z.Y. Zhao, B.G. Zhao, Y.H. He, and W.Y. Chen, Preparation and characterization of NASICON with a new sol-gel process, *Mater. Lett.*, 58(2003), No.1-2, p.226.

[15] H.Y. Dang and X.M. Guo, Investigation of porous counter electrode for the CO_2 sensing properties of NASICON-based gas sensor, *Solid State Ionics*, 201(2011), No.1, p.68.

[16] F.S. Baumann, J. Fleig, H.U. Habermeier, and J. Maier, Impedance spectroscopic study on well-defined (La,Sr)-(Co,Fe)$O_{3-\delta}$ model electrodes, *Solid State Ionics*, 177(2006), No.11-12, p.1071.

[17] H. Aono, N. Imanaka, and G.Y. Adachi, High Li^+ conducting ceramics, *Acc. Chem. Res.*, 27(1994), No. 9, p.265.

[18] J.S. Lee, C.M. Chang, Y.I. Lee, J.H. Lee, and S.H. Hong, Spark plasma sintering (SPS) of NASICON ceramics, *J. Am. Ceram. Soc.*, 87(2004), No.2, p.305.

[19] H.Y. Dang and X.M. Guo, Characteristics of NASICON-based thick-film CO_2 sensor attached with integrated auxiliary electrode, *IEEE Sens. J.*, 12(2012), No.7, p.2430.

[20] S. Yde-Andersen, J.S. Lundsgaard, L. Møller, and J. Engell, Properties of NASICON electrolytes prepared from alkoxide derived gels: ionic conductivity, durability in molten sodium and strength test data, *Solid State Ionics*, 14(1984), No.1, p.73.

[21] W. Bogusz, F. Krok, and W. Piszczatowski, Particular features of admittance spectra of polycrystalline NASICON samples, *Solid State Ionics*, 119(1999), No.1-4, p.165.

[22] E. Traversa, H. Aono, Y. Sadaoka, and L. Montanaro, Electrical properties of sol-gel processed NASICON having new compositions, *Sens. Actuators B*, 65(2000), No.1, p.204.

[23] A. Essoumhi, C. Favotto, M. Mansori, and P. Satre, Synthesis and characterization of a NASICON series with general formula $Na_{2.8}Zr_{2-y}Si_{1.8-4y}P_{1.2+4y}O_{12}$ ($0\leq y\leq 0.45$), *J. Solid State Chem.*, 177(2004), No.12, p.4475.